RSC Advances

ROYAL SOCIETY OF CHEMISTRY

www.rsc.org/advances

Surface modification of cellulose scaffold with polypyrrole for the fabrication of flexible supercapacitor electrode with enhanced capacitance

Shilin Liu[a*], Kuan He[a], Xia Wu[a], Xiaogang Luo[b], Bin Li[a]

a. College of Food Science & Technology, Huazhong Agricultural University, Wuhan, Hubei, 430070, China;

b. Key Laboratory of Green Chemical Process of Ministry of Education, School of Chemical Engineering and Pharmacy, Wuhan Institute of Technology, Wuhan 430073, China.

[*]Corresponding author: slliu2013@mail.hzau.edu.cn (S. Liu).

Abstract

Surface modification of cellulose scaffold for the preparation of flexible conductive composite has been carried out by using template-polymerization method. The effects of the concentration of the pyrrole, reaction time on the structure and properties of the composites have been investigated. The as-prepared polypyrrole/cellulose integrated the merits of cellulose and conductive polypyrrole (Ppy), the structurally defined Ppy/cellulose composites exhibited electrical conductivity as high as 0.59 $S \bullet cm^{-1}$ with Ppy content only about 28.89 wt%. Furthermore, it was foldable and could be used as flexible electrode for supercapacitors. The specific capacitance of the CPy-005 was about 392-308 $F \bullet g^{-1}$ at a current density ranging from 0.1 to 0.4 $A \bullet g^{-1}$, which kept high stability during the charge-discharge cycle, and the capacity was decreased only 18% after 1000 cycles at current density of 0.4 $A \bullet g^{-1}$. The unique porous bulk structure and rough surface properties enabled the construction of cellulose based on flexible supercapacitors with a reasonably good performance and a low price, which would provide a candidate for the future "green" and "once-use-and-throw-away" electronics.

Keywords: cellulose, energy storage devices, conductive materials, supercapacitor

Introduction

The integration of natural materials with electronic elements forms multifunctional devices has been the subject of intense scientific research recently, and "cellulose based flexible supercapacitors" is an exciting area of cross-disciplinary research field currently emerged.[1-4] It has been reported that electroactive paper with improved bending displacement was fabricated by coating Ppy on cellophane.[5] Electronic modification of cellulose particles could be prepared by blending cellulose whiskers suspension[6,7] or cellulose solution[8] with polyaniline solution or a dipping of microfibrillated cellulose aerogel in a polyaniline solution.[9,10] Significant efforts have also been carried out to design cellulose based on flexible supercapacitor electrodes through chemical polymerization of conductive polymers on the cellulose pulp suspension,[11] pulp fibers,[12] microfibrillated cellulose,[13] individual cellulose fibers[14] and bacterial cellulose nanofibrils.[15-17] Recently, poly(ethylenedioxythiphene) (PEDOT) coated cellulose electrodes have been shown and exhibited a specific volumetric capacitance of 145 $F \cdot cm^{-3}$ at 0.4 $mA \cdot cm^{-2}$ when normalized the volume of the active material.[18] Flexible polyaniline/Au/paper has been found to exhibit a volumetric capacitance of 800 $F \cdot cm^{-3}$ at 1 $mA \cdot cm^{-2}$ based on the volume of the active polyaniline layer.[19] However, the extensive progress in the development of cellulose-based electrodes was not able to compete with carbon and carbides electrodes regarding conductivity and volumetric capacitance. Questing for sustainable and inexpensive cellulose-based electrodes with high conductivity and volumetric capacitance therefore still constitutes a challenge.

We have put an intensive research on cellulose dissolving and construction of functional cellulose materials from the developed solvents. In our previous work, aqueous solvents containing alkaline and urea have been developed for cellulose dissolving.[20,21] The regenerated cellulose films prepared from LiOH/urea or NaOH/urea aqueous solution had porous structure, which could be used as scaffolds for the in-situ synthesis of inorganic nanoparticles,[22-24] and curable organic prepolymers[25,26] for the construction of functional cellulose materials. Recently, we have prepared conductive cellulose materials by using aniline monomer and porous structured cellulose scaffolds through in-situ polymerization, and found that the composites with polyaniline content about only 24.6 wt% exhibited electrical conductivity as high as 0.06 $S \bullet cm^{-1}$ and a specific capacitance of 120-160 $F \bullet g^{-1}$ in the supercapacitor.[27] In order to obtain the high capacities required for efficient extractions of ions and the fast charging-discharging needed in cellulose-based energy storage devices, the cellulose scaffolds in the conducting polymer composites must clearly serve the dual purpose of mechanically reinforcing the brittle conductive polymers and enhancing the specific charge capacity by providing a continuous 3-D scaffold of high porosity. In this work, porous structured conductive cellulose composites were prepared by in-situ polymerization of pyrrole in the cellulose scaffolds to obtain highly electroactive cellulose composites with large surface areas. The described manufacturing process was entirely water-based and did not include any time-consuming solvent-exchange and drying steps to retain the large surface area of hydrogels upon water removal. It was shown that the obtained composites have

surface areas that more than 30 m^2/g with Ppy content less than 30 wt%, which rendered it well-suited for use in applications for supercapacitors. The specific capacitance of the CPy-005 was about 392-308 $F•g^{-1}$ at a current density ranging from 0.1 to 0.4 $A•g^{-1}$ in the supercapacitor, it had high stability during the charge-discharge cycle, and the capacity was only decreased to 82% after 1000 cycles at current density of 0.2 $A•g^{-1}$. The present work shed light on the design of green flexible supercapacitors based on low-cost and environmentally friendly nature of cellulose as well as simple fabrication techniques, which would have promising candidates for the future "green electronics".

Experimental section

Chemicals

Cotton linter pulp was provided by Hubei Chemical Fiber Group Ltd (α-cellulose > 95%, viscosity-average molecular weight was 1.03×10^5, Xiangfan, China). Other chemicals with analytical grade were supplied by the Sinopharm Chemical Reagent Co. Ltd (China) and used without further purification.

Preparation of porous structured Ppy/cellulose composites

The dissolving process for cellulose has been reported in our previous work. Briefly, Cotton linter pulp (native cellulose) was dispersed into aqueous LiOH/urea solution, and froze at -20 ^oC, then, it was thawed at room temperature to obtain a transparent cellulose solution (5 wt%). After the removal of the bubbles in the solution by centrifugation, the solution was cast on a glass plate with the thickness about 1 mm, and then immersed it into anhydrous ethanol for coagulation and regeneration. The

RC films were washed with deionized water thoroughly and subsequently immersed them into $FeCl_3$ solution for 3 hours. Pyrrole monomer was added into it and kept the reaction at 0 ^oC for 4 hours. In this process, the pyrrole monomer could permeate into the cellulose scaffolds through diffusion, and oxidized polymerization was happed in the cellulose matrix, the color of the RC films turned from colorless into black. The ratio of Pyrrole and $FeCl_3$ was controlled to be 1 : 2. The composite hydrogels were washed with deionized water thoroughly, and then replaced the water with ethanol, and dried with supercritical CO_2 method. The composites prepared from pyrrole with concentration of 0.01, 0.02, 0.03, 0.04, 0.05 and 0.06 mol•L^{-1} was coded as CPy-001, CPy-002, CPy-003, CPy-004, CPy-005 and CPy-006, respectively.

Characterization

Fourier-transform infrared (FT-IR) spectroscopies of the samples were characterized with an FT-IR spectrometer (FT-IR 615, Japan). The samples were grounded into powders and dried in a vacuum drying oven at 50 ℃ for 36 h, then mixed with KBr, and pressed for the tests. X-ray diffractometry tests were carried out on reflection mode (Rigaku RINT 2000, Japan) with Ni-filtered CuKa radiation. Thermal gravimetric analysis (TGA) was carried out on the thermogravimetric analysis (Ulvac TGD 9600). The samples were cut into powders and about 30 mg of the powder was placed in a platinum pan and heated from 20 to 700 ^oC at a rate of 10 k•min^{-1} in nitrogen atmosphere. Scanning electron microscopy (SEM) observation was carried out by using a Hitachi S-4800 microscope. Before being analyzed, samples were cut into small pieces from the prepared samples and coated with a thin

layer of evaporated gold. The mechanical properties of the samples at wet state were characterized with a tensile tester (CMT 6503, Shenzhen SANS Test machine Co. Ltd, China) according to ASTM/D638-91, the crosshead speed was kept constant at 1 $mm•min^{-1}$. The conductivity of the samples was characterized with a conventional four-point probe technique (RTS-8, Probes Tech., China) at 25 ^{o}C. According to the four point probe method, resistivity could be calculated with $\rho = 2\pi s (V / I)$, where S was the distance between the probes (mm), which was kept constant, I was the supplied current in microamperes, and the corresponding voltage was measured in millivolts. Conductivity was calculated by using $\sigma = 1/(\rho•X)$. In this process, five replicates for each sample were performed to obtain an average value.

Cyclic voltammetry and chronopotentiometry were carried out on a CHI660D electrochemical work station (Shanghai, China). Conventional three-electrode system was employed, involving glass carbon electrode as the working electrode, a platinum wire as the counter electrode and a saturated calomel electrode (SCE) as the reference electrode. The composite electrodes were prepared by dropcasting certain amounts of the dispersions on glassy carbon electrodes (dried at 40 °C). Cyclic voltammetry was performed in the voltage range from -0.7 to 1.0 V at 5, 10, 20, and 30 $mV•s^{-1}$ scan rates in 1 $mol•L^{-1}$ NaCl. The galvanostatic charge-discharge experiment was carried out in the potential range from -0.7 to 1.0 V with an applied current density of 0.1, 0.2, and 0.4 $A•g^{-1}$. The working electrode was prepared by mixing the active material with 15 wt% acetylene blank and 5 wt% polytetrafluoroeyhylene (based on the total electrode mass) to form a slurry. Then the slurry was cast on stainless steel mesh.

Galvanostatic charge-discharge curves were measured in the potential range of -0.7-1.0 V at different current density. In this process, the composites were used as working electrode, and platinum foil (1 cm×1 cm) and a saturated calomel electrode (SCE) were used as the counter and reference electrode, respectively. The electrochemical measurements were carried out in a 1.0 mol/L NaCl aqueous electrolyte at room temperature.

Results and discussion

Figure 1 shows the SEM images of the pure RC and composites. The RC had porous structure, comprising of fibrils with the diameter about 20 nm, as it was shown in Figure 1a. The porous structure was resulted from the phase separation of the cellulose solution during the regeneration process, where cellulose-rich and solvent-rich regions were formed, and the solvent-rich regions contributed to the formation of the pores. The cellulose aerogel had porosity about 92%, and the S_{BET} was about 270 $m^2 \bullet g^{-1}$. It could draw the following conclusions that the RC hydrogel film before freeze drying had porous structure. When the RC hydrogel film was immersed into pyrrole solution, the pyrrole could penetrate into the porous structured cellulose hydrogel through diffusion. The large amount of hydroxyl groups of cellulose could interact with amine groups of pyrrole to form the hydrogen bands which ensured the uniform distribution of pyrrole around the cellulose nanofibrils. The interaction between the pyrrole and cellulose nanofibrils was a physical nature without involving chemical reaction. The pyrrole was polymerized in the cellulose matrix when $FeCl_3$ solution was added. The color of the cellulose hydrogel turned

from colorless into black, indicating the successful incorporation of Ppy in the RC scaffolds. Figure 1b-f shows the surface images of the Ppy/cellulose composites. The concentration of the pyrrole monomers had an obvious influence on the morphology of the composites. For the composites prepared from 0.01 mol•L^{-1} pyrrole, the cellulose nanofibrils were covered with continuous sheath of Ppy, and some Ppy particles were formed on the surface of the composites, as it was shown in Figure 1b. This process would be called templated polymerization, where the pyrrole was polymerized in the cellulose scaffolds connected to form a continuous sheath by taking the cellulose nanofibrils as templates. It was needed to note that there was no Ppy precipitated from the reaction system when the color of the RC films turned into black. When the concentration of the pyrrole was increased to 0.02 mol•L^{-1}, the composites exhibited a different morphology when compared with that of CPy-001, as it was shown in Figure 1c. When the concentration of pyrrole was further increased, the content of Ppy particles with particle size about 100 nm increased with the precipitation or aggregation forming on the surface of the composites (Figure 1d-f). It was well known that the major drawback of the conductive polymers (e.g. polyaniline, Polypyrrole, etc) was the unprocessability and intractability which had made their processing into the desired form was rather difficult, while in our research, the cellulose nanofibrils could work as a good templates to assist the formation Ppy coatings around cellulose nanofibrils, which made it possible to prepare the conductive composites with different dimensions.

Based on the results from Figure 1, the influence of the reaction time on the

187 structure of the Ppy/cellulose composites has been investigated. Figure 2 shows the
188 images of the composites prepared from different reaction time with pyrrole
189 concentration of 0.05 mol•L^{-1}. The porous structured RC scaffolds were filled with the
190 Ppy particles within 1 h, as it was shown in Figure 2b, it demonstrated that the
191 polymerization reaction was quickly, which was important for the large-scale
192 preparation and practical application of the cellulose based conductive materials. With
193 a longer reaction time, precipitation or aggregation of the Ppy colloidal particles
194 occurred to form larger dimension particles on the surface of the composites (Figure
195 2e, f). The composites prepared from longer polymerization time exhibited a rougher
196 surface, and the microstructure of the composites could be controlled by changing the
197 concentration of the pyrrole monomer or the polymerization time. The S_{BET} inferred
198 from the N_2 adsorption isotherms of the composites prepared from reaction time of 1,
199 1.5, 2.0, 2.5 and 4.0 h was about 66, 71, 43, 41 and 30 m^2•g^{-1}, respectively.

200 We also characterized the molecular structure of the resultant Ppy layer in the
201 composites, as it was shown in Figure 3. In the case of pure RC, a broad band at 3403
202 cm^{-1} was attributed to O-H stretching vibration. The band at 2897 cm^{-1} represented the
203 aliphatic C-H stretching vibration. A sharp and steep band which was observed at
204 1068 cm^{-1} was due to the presence of C-O-C stretching vibrations.[28] In the case of
205 Ppy/cellulose composites, the band at 3403 and 1647 cm^{-1} became weaker with the
206 increasing of the content of Ppy. The absorption band at 1548 cm^{-1} was assigned to
207 the pyrrole ring, e.g. the combination of C-C and C=C stretching vibrations, and the
208 band at 1372 cm^{-1} was associated with C–N stretching vibration.[29] The band at 922

209 cm^{-1} was assigned to C=C in-plane bending vibrations of the pyrrole ring. These
210 characteristic bands confirmed the formation of PPy.

211 Figure 4 shows the XRD of the RC and Ppy/cellulose composites. The peaks at 2θ
212 = 12.1, 20.3, and 21.8° were corresponded to the (1$\bar{1}$0), (110), and (200) planes of
213 cellulose II crystalline, respectively.[30] An abroad asymmetric scattering peak of
214 typical amorphous PPy was shown in the XRD patterns, the center of the peaks was
215 located at 2θ = 26°, which was similar to those of the PPy prepared by ordinary
216 chemical oxidation methods.[31,32] It was noted that in addition to the peaks of cellulose
217 II, it was difficult to detect the peak of Ppy in the composites. The chemical structure
218 of RC was remained unchanged by the coating of amorphous Ppy shell, suggesting
219 the polymerization happened in the pyrrole monomers, and the cellulose scaffolds was
220 just as templates for the stabilization of the synthesized Ppy particles. It was worth
221 noting that the porous structured RC scaffolds was a fascinating template for the
222 construction of functional materials through in-situ polymerization of polymer
223 monomers, besides for the synthesis of inorganic nanoparticles or cured some organic
224 prepolymers in situ.

225 BET measurements were performed to measure the surface areas of the composites.
226 The samples were characterized by using nitrogen adsorption and desorption
227 isotherms at 77 K, and the result was shown in Figure 5. The sharp nitrogen uptake
228 near P^0 indicated a continuity of the pore size distribution between mesopores and
229 macropores (diameter larger than 50 nm), thus the presence of both meso and
230 macro-porosities in the composites.[33,34] S_{BET} inferred from the N_2 adsorption

isotherms by a Brunauer-Emmett-Teller analysis of the amount of gas adsorbed at P/P^0 between 0.05 and 0.3 was about 36, 34, 36, 33, 30, and 28 $m^2 \bullet g^{-1}$ for CPy-001, CPy-002, CPy-003, CPy-004, CPy-005, and CPy-006, respectively. It indicated that the composites had a larger surface area. In addition, the observed hysteresis loop shifts to a higher relative pressure on approaching $P/P^0 \approx 1$, which suggested that macropores (size > 50 nm) were also presented. This shift was confirmed by the corresponding pore-size distribution that showed two peaks for mesopores along with macropores up to 50 nm in size (Figure. 6). This structure could provide low-resistant pathways for the ions through the porous structure, and shorter diffusion routes could be formed because of the ordered mesoporous channels. The larger mesoporous structure (20-50 nm) was a consequence of the interconnected network. Maintaining such a macro/mesoporous structure could potentially provide enhanced electrolyte access to the high interfacial areas where would improve the charge transport and power capability. Moreover, ion-buffering reservoirs formed in the larger mesopores could reduce the diffusion distances to the interior surfaces. Such hierarchically connected pore structures of the conductive composites could facilitate the penetration of electrolytes in the matrix, providing convenient channels for electrolyte ion transportation, and electroactive sites for fast energy storage at large current densities. These properties were important for supercapacitor electrode materials with a large specific capacitance and high-rate charge-discharge ability.

The thermal stability of the RC and the Ppy/cellulose composites was shown in Figure 7a. All the samples exhibited excellent heat-resistance up to at least 200 °C.

There was a small weight loss of ~5 wt% below 100 ^{o}C for the RC and composites, which was ascribed to the release of the moisture from the samples. With the elevating temperature, the pure RC film showed an obvious weight loss in the temperature about 300~350 ^{o}C, it was the decomposition temperature of cellulose in N_2. The composites experienced a sharp weight loss from 200 to 350 ^{o}C, and the TGA curves for the composites were different with the increasing the content of the Ppy in the composites. Ppy was known to degrade in a three-step process, where water left from the sample first and thereafter a degradation process involving the counter ions follows, and finally, the polymer backbone was degraded.[35,36] It was also seen in the TGA curves that the composites followed the first process of the Ppy before the main cellulose degradation and after which it followed the second degradation process of Ppy. This confirmed the presence of both cellulose and Ppy in the composites. When the temperature was increased to 400 °C, the TGA curves followed that of the RC sample with a small shift in weight percentage corresponding to the residuals presented in the composite material. The mass fraction of Ppy in the composites was calculated by considering the extent of decomposition of cellulose and Ppy at 800 °C and it was shown in Figure 8a. For the practical application, the composites was used to absorb electrolytes, therefore, the tensile stress-strain behavior of Ppy/cellulose composites at wet state were characterized and shown in Figure 7b. It indicated that the tensile strength decreased with the amount of Ppy in the composites. This decreased in tensile strength of the Ppy/cellulose composites might be related to the weakened inter- and intramolecular hydrogen bonding of cellulose was caused by the

introduction of Ppy. It was important to note that the tensile curve of pure Ppy was not shown due to the poor mechanical properties of Ppy powders and the brittleness of the Ppy film. In addition, it was possible to bend the Ppy/cellulose composites to angles of about 180^{o} without breaking, as it was shown in the inserted photo in Figure 7b. It was obvious that the composites overcame the limitation of the preparation of conductive film from pure Ppy, and it was foldable, and had good mechanical properties, these characteristics made it as a promising material in the application in electrically conductive flexible film fields.

The electrical conductivity of Ppy/cellulose composites was optimized by sequentially fine tuning the reaction parameters including the concentration of the pyrrole monomer, polymerization time. Figure 8a shows the effects of the concentration of pyrrole monomer on the Ppy content and the conductivity of the composites. The concentration of the pyrrole monomers had an obvious influence on the conductivity of the composites, and it demonstrated that the conductivity of the composites was correlated to the content of Ppy. For the composites prepared from pyrrole monomer with concentration of 0.02 mol•L^{-1}, the conductivity of the composites was about 3.18×10^{-4} S•cm^{-1}, and the content of the Ppy was about 13.19 wt%. When the concentration of the pyrrole monomer was up to 0.06 mol•L^{-1}, the Ppy content in the composites was increased to 28.89 wt% and the conductivity was increased to 0.59 S•cm^{-1}. It must be noted that the conductivity of insulating materials including most thermosets and wood materials is in the range of 1×10^{-16} to 1×10^{-12} S•cm^{-1}. Some researchers have explored the preparation of Ppy/cellulose composites

with conductivity about 1.5 ~ 2.5 S•cm^{-1}, while the content of Ppy in the composites was in the range of 58wt% ~70 wt%.[37, 38] In our work, we also found that the conductivity of the composites could be improved by increasing the content of the content of Ppy, however, the composites would be brittle and the mechanical performance of the composites would be decreased with higher content of Ppy. Therefore, the higher concentration of pyrrole used in our study was 0.05 mol•L^{-1}. The influence of reaction time on the conductivity of the composites prepared from pyrrole with concentration of 0.05 mol•L^{-1} was shown in Figure 8b. The conductivity of the composites was 0.44 S•cm^{-1} for the reaction time of 1 h, and it was decreased to about 0.38 S•cm^{-1} for the reaction time increasing to 4 h. It was probably ascribed to the homogeneous of the Ppy coating formed in the cellulose matrix, as it was shown in Figure 2. It indicated that the conductivity of the composites was not only affected by the content of the Ppy, but also was influence by the homogeneous distribution of the formed Ppy coating.

Cyclic voltammetry is considered to be an ideal tool to test the capacitive behavior of electronic material, and a large magnitude of current and a rectangular type of voltammogram are indications of ideal capacitive nature of a material. Figure 9a shows the CVs of the Ppy/celluloses prepared from different concentration of pyrrole monomers. It was found that the CV curve area of Ppy/cellulose composites increased with the increasing the content of Ppy. The presence of cellulose as a template in the polymerization system could result in the change in the morphology of Ppy, and the cellulose itself did not contribute to the electrical capability. Therefore, the increased

CV curve area was resulted from the large amount of Ppy components, contributing to transfer of electrons and gathering the charge. The redox reaction peak that was responsible for the pseudocapacitive behavior was clearly seen, and the redox peaks are slightly shifted due to the different nanostructures. It was seen that as the conductivity of the composites increased, the integrated current under the curve increased. To estimate the ion-exchange capacity of the composites, the charge capacity was calculated by integrating the current vs time curve from the anodic scanned in the voltammogram. The obtained supercapacitance values at 20 mV• s^{-1} were 245, 276, 347 and 385 F• g^{-1} for CPy-003, CPy-004, CPy-005, and CPy-006, respectively. Although the specific capacitance still fell behand the theoretical value (620 F• g^{-1}),[39] it was superior or at least comparable to most previous reports, such as 172-197 F• g^{-1} for Ppy nanotubes synthesized using methyl orange (MO)/$FeCl_3$,[40,41] 305 F•g^{-1} for Ppy nanowires prepared using cetyltrimethylammonium bromide (CATB)[42] and 586 F•g^{-1} for Porous polypyrrole clusters prepared by electropolymerization.[43] The value reports in the present work was due to the structural characteristics of composites, which were able to provide (1) proper pore configuration after the Ppy deposited onto the cellulose scaffolds and its open porosity structure with a high specific surface area, (2) the interconnected three dimensional composites with high conductivity for fast charge was transferred from the reversible Faradiac reaction, and (3) hydrophilic properties with low-resistant pathways for the ions.

The CV response of CPy-003 at scan rates from 5 to 30 mV• s^{-1} within the potential

window of -0.7 to 1.0 V was shown in Figure 9b. The voltammetric currents were directly proportional to the scan rate, indicating an ideally capacitive behavior.[44-46] The profiles of specific capacitance of CPy-003 against the scan rate was decreased from 316 to 208 $F \bullet g^{-1}$ with the scan rates increasing from 5 to 30 $mV \bullet s^{-1}$. Such a decrease in capacitance with scan rate was attributed to the presence of inner active sites that cannot complete the redox transitions at higher scan rates. These incomplete redox transitions were probably due to the diffusion effect of ions within the electrode. The decreasing capacitance suggested that parts of the electrode surface were inaccessible at high charging-discharging rates. Hence, the specific capacitance obtained at the slowest scan rate was thought to be the fullest utilization of the electrode material.

Figure 10a shows the galvanostatic charging-discharging plots of the CPy-005 at various current densities of 0.1, 0.2, and 0.4 $A \bullet g^{-1}$. The triangular symmetry and linear slopes confirmed the good pseudocapacitive behavior for the CPy-005 again. The specific capacitance of the electrode could be calculated using the following equation:[47]

$$C_m = \left(It\right) \Big/ \left(\mathrm{V}Vm\right)$$

Where C_m was specific capacitance ($F \bullet g^{-1}$), I was charge/discharge current (A), t was the time of discharge (S), ΔV was the voltage difference between the upper and lower potential limits, and m was the mass of the active electrode material. According to the above equation, the gravimetric capacitance of the PCy-005 at various current densities was plotted in Figure 10b. A decreasing specific capacitance from 392 to 308

363 F• g^{-1} at an increasing current density from 0.1 to 0.4 A•g^{-1} was observed. The charge
364 storage mechanism was based on the fast and reversible doping/undoping of PPy with
365 Cl^- ions, and it could be written as:

366 $$[PPy^+]Cl^- + e^- \leftrightarrow [PPy^0] + Cl^-$$

367 Hence, the reduced capacitance at higher current density was ascribed to the limited
368 diffusion time of electrolyte ions into the interior surfaces of composites, Still, the
369 specific capacitance of the composites was as high as 308 F• g^{-1} at a high current
370 density of 0.4 A•g^{-1}. The high surface area and an easy path for intercalation and
371 de-intercalation of Cl^- ions reduced the internal resistance of the electrode.

372 The long cycle life of supercapacitors was also a crucial parameter for the practical
373 application. Figure 11a shows the typical galvanostatic charge-discharge tests of the
374 PCy-005 composite electrode at a current density of 0.4 F•g^{-1}. The charge curves were
375 symmetric to their corresponding discharge counterparts in the potential window,
376 which indicated the feasibility of the CPy-005 electrode system for the development
377 of supercapacitors. The discharge specific capacitance of the CPy-005 composite
378 electrode was up to 308 F•g^{-1} at a current density of 0.4 A•g^{-1}. Moreover, cyclic
379 performances of the CPy-005 composite electrode were also examined by
380 galvanostatic charge-discharge tests for 1000 cycles. Figure 11b shows the
381 capacitance kept at least about 82% after 1000 cycles at current density of 0.4 A•g^{-1}.
382 The results demonstrated that the CPy-005 composite electrode offered an excellent
383 pseudocapacitance performance, including high specific capacitance and rate
384 capability, good charge-discharge stability of the electrode. This should be attributed

to form a more uniform coating of the Ppy layer on the porous structured cellulose scaffolds (rather than highly agglomerated structure), which affected the electrode's conductivity and its electrochemical capacitance positively. To expand our investigation further, we have prepared metal oxide/Ppy/cellulose composite aerogel electrodes by adopting electro-polymerization of pyrrole on the inorganic/cellulose composites, and identically assessed. As is expected, the composites electrodes demonstrated an excellent cycle life, high capacity and superiority to Ppy/cellulose electrodes in all aspects.

Conclusions

Highly flexible, porous structured conductive Ppy/cellulose aerogel based electrode with excellent electro-chemical performance was presented. The significantly improved properties were related mainly to the low density, high flexibility, hierarchical structure of the cellulose scaffold, and the well-connected 3D core-shell structure of the Ppy/celluloses. The conductive Ppy layer facilitated efficient charge transfer during the charge-discharge process. The Ppy/celluloses exhibited electrical conductivity as high as 0.59 $S \bullet cm^{-1}$ with Ppy content only about 28.89 wt%. Furthermore, it was foldable and could be used as flexible electrode for supercapacitors. The specific capacitance of the composites was about 392-308 $F \bullet g^{-1}$ at a current density ranging from 0.1 to 0.4 $A \bullet g^{-1}$ in the supercapacitor, it kept high stability during the charge-discharge cycle. The 3D electrode architecture is very promising for flexible and lightweight energy storage application. This cellulose scaffolds is not only appropriate for the present electrodes, but also may be used in

407 green electronics for a range of applications where lightweight, flexibility and
408 environmentally safe and/or biocompatible are important.

409 **Acknowledgements**

410 This work was supported by the National Natural Science Foundation of China (No.
411 51273085 and 51003043), and the National Key Technology R&D Program
412 (2015BAD16B06), and the project (2014PY024) by the Fundamental Research Funds
413 for the Central Universities.

414

Notes and references

1 Y. H. Jung, T. Chang, H. Zhang, C. Yao, Q. Zheng, V. W. Yang, H. Mi, M. Kim, S. J. Cho, D. W. Park, H. Jiang, J. Lee, Y. Qiu, W. Zhou, Z. Cai, S. Gong and Z. Ma, *Nat. Commun*., 2015, **6**, 7170-7180.

2 J. Huang, H. Zhu, Y. Chen, C. Preston, K. Rohrbach, J. Cumings and L. Hu, *ACS Nano*., 2013, **7**, 2106–2113.

3 Y-Z. Zhang, Y. Wang, T. Cheng, W-Y. Lai, H. Pang and W. Huang, *Chem Soc Rev*., 2015, **44**, 5181-5199.

4 M. Irimia-Vladu, *Chem Soc Rev*. 2014, **43**, 588-610.

5 S. Deshpande, J. Kim and S.-R. Yun, *Smart Mater. Struct*., 2005, **14**, 876-880.

6 E. Tkalya, M. Ghislandi, W. Thielemans, P. van der Schoot, G. de With and C. Koning, *ACS Macro Lett*., 2013, **2**, 157-163.

7 Y. Gu and J. Huang, *Colloids Surf. A.*, 2013, **433**, 166-172.

8 X. Shi, L. Zhang, J. Cai, G. Cheng, H. Zhang, J. Li and X. Wang, *Macromolecules*., 2011, **44**, 4565-4568.

9 X. Zhang, Z. Lin, B. Chen, W. Zhang, S. Sharma, W. Gu and Y. Deng, *J. Power Sources.*, 2014, **246**, 283-289.

10 M. Pääkkö, J. Vapaavuori, R. Silvennoinen, H. Kosonen, M. Ankerfors, T. Lindström, L. A. Berglund and O. Ikkala, *Soft Matter.*, 2008, **4**, 2492-2499.

11 X. Qian, J. Shen, G. Yu and X. An, *Bioresources*., 2010, **5**, 899-907.

12 F. M. Kelly, J. H. Johnston, T. Borrmann and M. J. Richardson, *Eur. J. Inorg. Chem*., 2007, **35**, 5571-5577.

13 M. L. Auad, T. Richardson, W. J. Orts, E. S. Medeiros, L. H. Mattoso, M. A. Mosiewicki, N. E. Marcovich and M. I. Aranguren, *Polym. Int.*, 2011, **60**, 743-750.

14 X. Liu, W. Zhou, X. Qian, J. Shen and X. An, *Carbohydr. Polym*., 2013, **92**, 659-661.

15 D. Müller, J. Mandelli, J. Marins, B. Soares, L. Porto, C. Rambo and G. Barra, *Cellulose*., 2012, **19**, 1645-1654.

16 B-H. Lee, H-J. Kim and H-S. Yang, *Curr. Appl. Phys*., 2012, **12**, 75-80.

17 W. Hu, S. Chen, Z. Yang, L. Liu and H. Wang, *J. Phys. Chem. B*., 2011, **115**, 8453-8457.

18 B. Anothumakkool, R. Soni, S. N. Bhange and S. Kurungot, *Energy Environ. Sci.*, 2015, **8**, 1339-1347.

19 L. Yuan, X. Xiao, T. Ding, J. Zhong, X. Zhang, Y. Shen, B. Hu, Y. Huang, J. Zhou and Z. L. Wang, *Angew. Chem*. 2012, **124**, 5018-5022.

20 S. Liu and L. Zhang, *Cellulose*., 2009, **16**, 189-198.

21 J. Zhou, S. Liu, J. Qi and L. Zhang, *J. Appl. Polym. Sci*., 2006, **101**, 3600-3608.

22 S. Liu, L. Zhang, J. Zhou and R. Wu, *J. Phys. Chem. C.*, 2008, **112**, 4538-4544.

23 S. Liu, L. Zhang, J. Zhou, J. Xiang, J. Sun and J. Guan, *Chem. Mater*., 2008, **20**, 3623-3628.

24 S. Liu, J. Zhou and L. Zhang, *J. Phys. Chem. C*, 2011, **115**, 3602-3611.

25 W. Li, Y. Wu, W. Liang, B. Li and S. Liu, *ACS Appl. Mater. Interfaces.*, 2014, **6**, 5726-5734.

26 S. Liu, D. Tao, T. Yu, H. Shu, R. Liu and X. Liu, *Cellulose*., 2013, **20**, 907-918.

27 S. Liu, T. Yu, Y. Wu, W. Li and B. Li, *RSC Adv*, 2014, **4**, 34134002D34143.

28 C. J. Grande, F. G. Torres, C. M. Gomez and M. Carmen Bañó, *Acta Biomater*., 2009, **5**, 1605-1615.

29 A. J. F. Romero, J. J. L. Cascales and T. F. Otero, *J. Phys. Chem. B.* 2005, **109**, 907-914.

30 L. Zhang, D. Ruan and J. Zhou, *Ind. Eng. Chem. Res*., 2001, **40**, 5923-5928.

31 J. Liu and M. Wan, *J. Mater. Chem*., 2001, **11**, 404-407.

32 P. Xu, X. Han, C. Wang, D. Zhou, Z. Lv, A. Wen, X. Wang and B. Zhang, *J. Phys. Chem. B*, 2008, **112**, 10443-10448.

33 A. Vinu, D. P. Sawant, K. Ariga, M. Hartmann and S. B. Halligudi, *Microporous Mesoporous Mater.*, 2005, **80**, 195-203

34 M. W. Xu, L. B. Kong, W. J. Zhou and H. L. Li, *J. Phys. Chem. C*, 2007, **111**, 19141-19147.

35 F. Mohammad, P. D. Calvert and N. C. Billingham, *Bull. Mater. Sci.*, 1995, **18**,

255-261.

36 P. M. Carrasco, M. Cortazar, E. Ochoteco, E. Calahorra and J. A. Pomposo, *Surf. Interface Anal.* 2007, **39**, 26-32.

37 G. Nyström, A. Mihranyan, A. Razaq, T. Lindström, L. Nyholm and M. Strømme, *J. Phys. Chem. B* , 2010, **114**, 4178-4182.

38 K. Jradi, B. Bideau, B. Chabot and C. Daneault, *J Mater Sci*., 2012, **47**, 3752-3762.

39 G. A. Snook, P. Kao and A. S. Best, *J. Power Sources*, 2011, **196**, 1-12.

40 J. H. Liu, J. W. An, Y. X. Ma, M. L. Li, R. B. Ma, M. Yu and S. M. Li, *Eur. Phys. J.: Appl. Phys.*, 2012, **57**, 30702-30710.

41 H. Mi, X. Zhang, X. Ye and S. Yang, *J. Power Sources*, 2008, **176**, 403-409.

42 Q. F. Wu, K. X. He, H. Y. Mi and X. G. Zhang, *Mater. Chem. Phys.*, 2007, **101**, 367-371.

43 D. P. Dubal, S. H. Lee, J. G. Kim, W. B. Kim and C. D. Lokhande, *J. Mater. Chem.*, 2012, **22**, 3044-3052.

44 D. P. Dubal, D. S. Dhawale, R. R. Salunkhe and C. D. Lokhande, *J. Electroanal. Chem*., 2010, **647**, 60-65.

45 C. Shi and I. Zhitomirsky, *Nanoscale Res. Lett.*, 2010, **5**, 518-523.

46 D. P. Dubal, D. S. Dhawale, R. R. Salunkhe, S. M. Pawar and C. D. Lokhande, *Appl. Surf. Sci*., 2010, **256**, 4411-3316.

47 A. L. M. Reddy and S. Ramaprabhu, *J. Phys. Chem. C*., 2007, **111**, 7727-7734.

497 **For table of content use only**

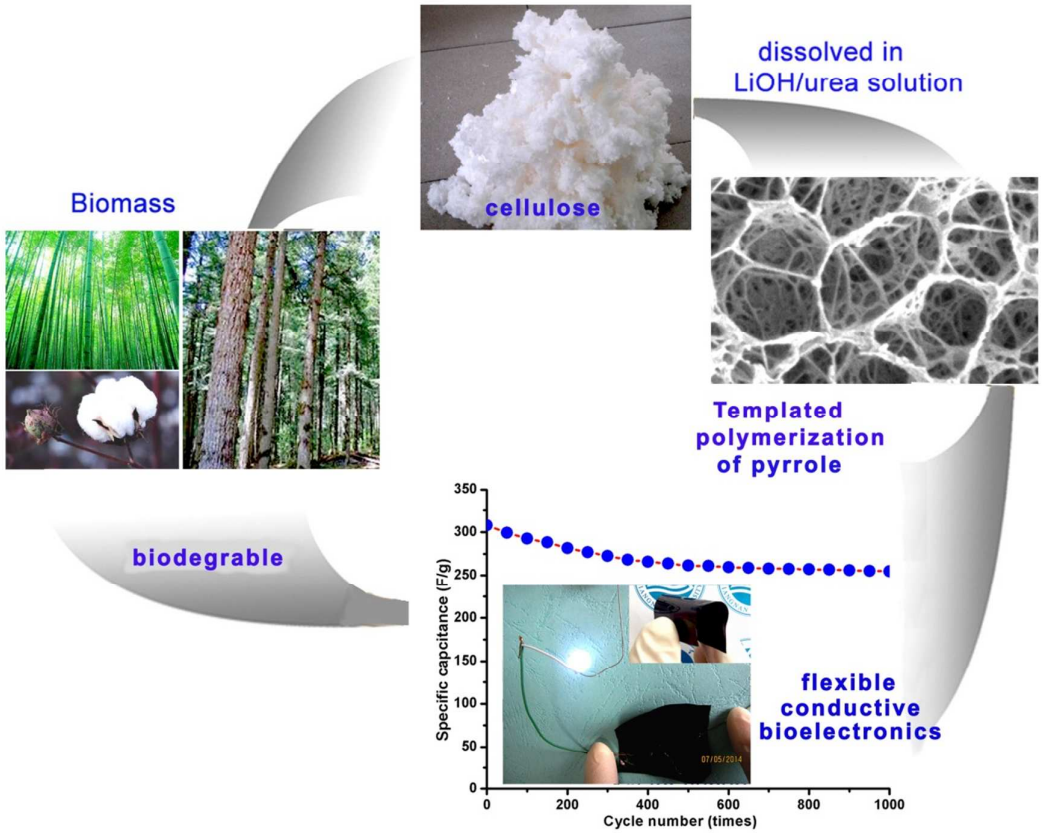

498

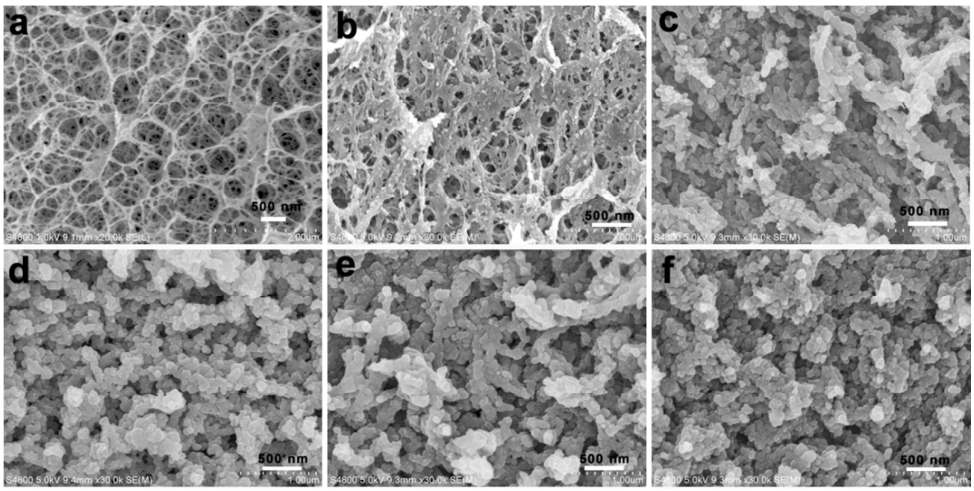

Fig 1 FE-SEM images of surface morphologies of the pure RC (a) and the Ppy/cellulose composites prepared from pyrrole with different concentration, (b) 0.01 mol•L^{-1}, (c) 0.02 mol•L^{-1}, (d) 0.03 mol•L^{-1}, (e) 0.04 mol•L^{-1}, and (f) 0.06 mol•L^{-1}, respectively.

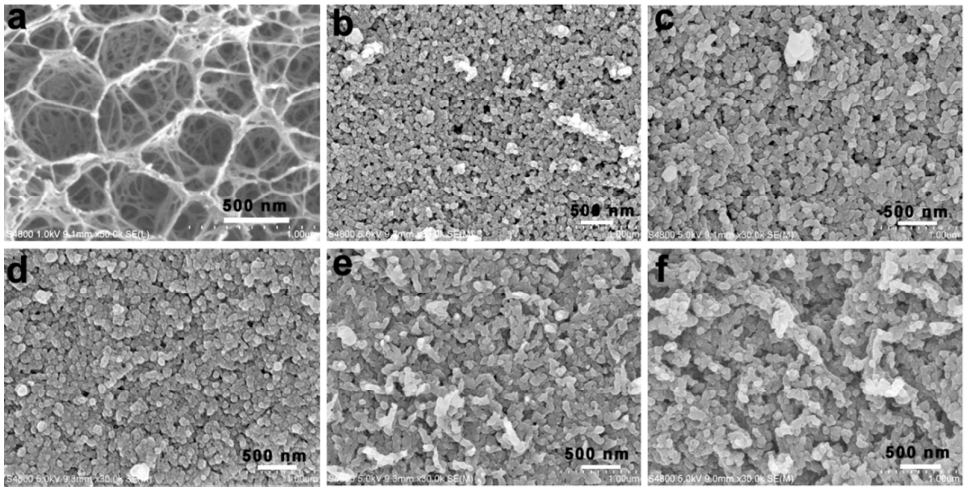

Fig. 2 FE-SEM images of the surface morphologies of the CPy-005 composites prepared from different reaction time, (a) 0 h, (b) 1 h, (c) 1.5 h, (d) 2h, (e) 2.5 h and (f) 4 h, respectively.

514

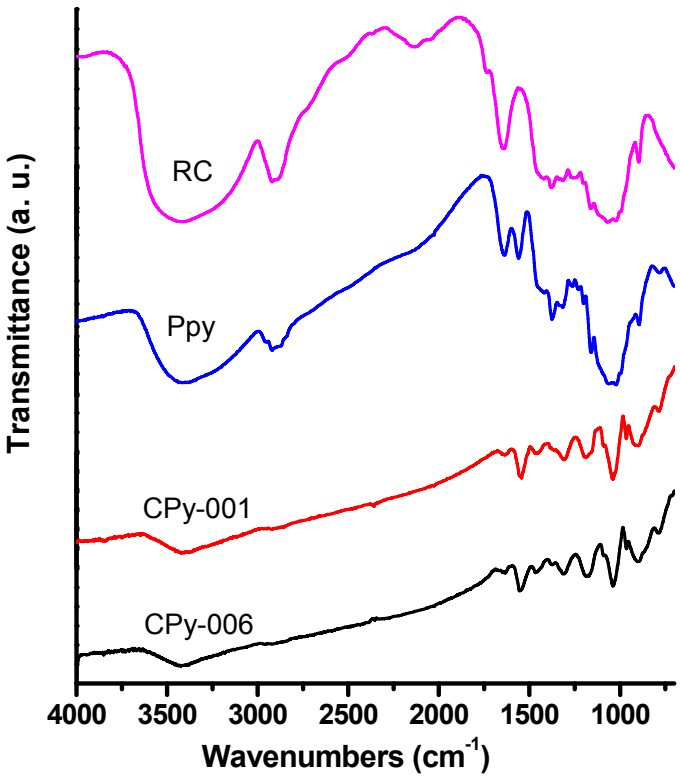

515

516 **Fig. 3** FT-IR spectra of pure RC, Ppy and some Ppy/cellulose composites.

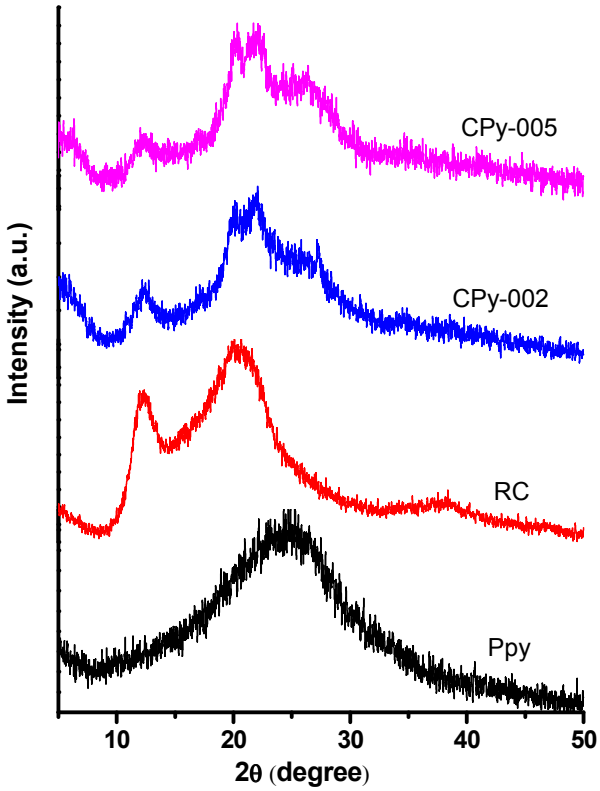

Fig. 4 XRD patterns of the RC, Ppy and Ppy/cellulose composites.

524

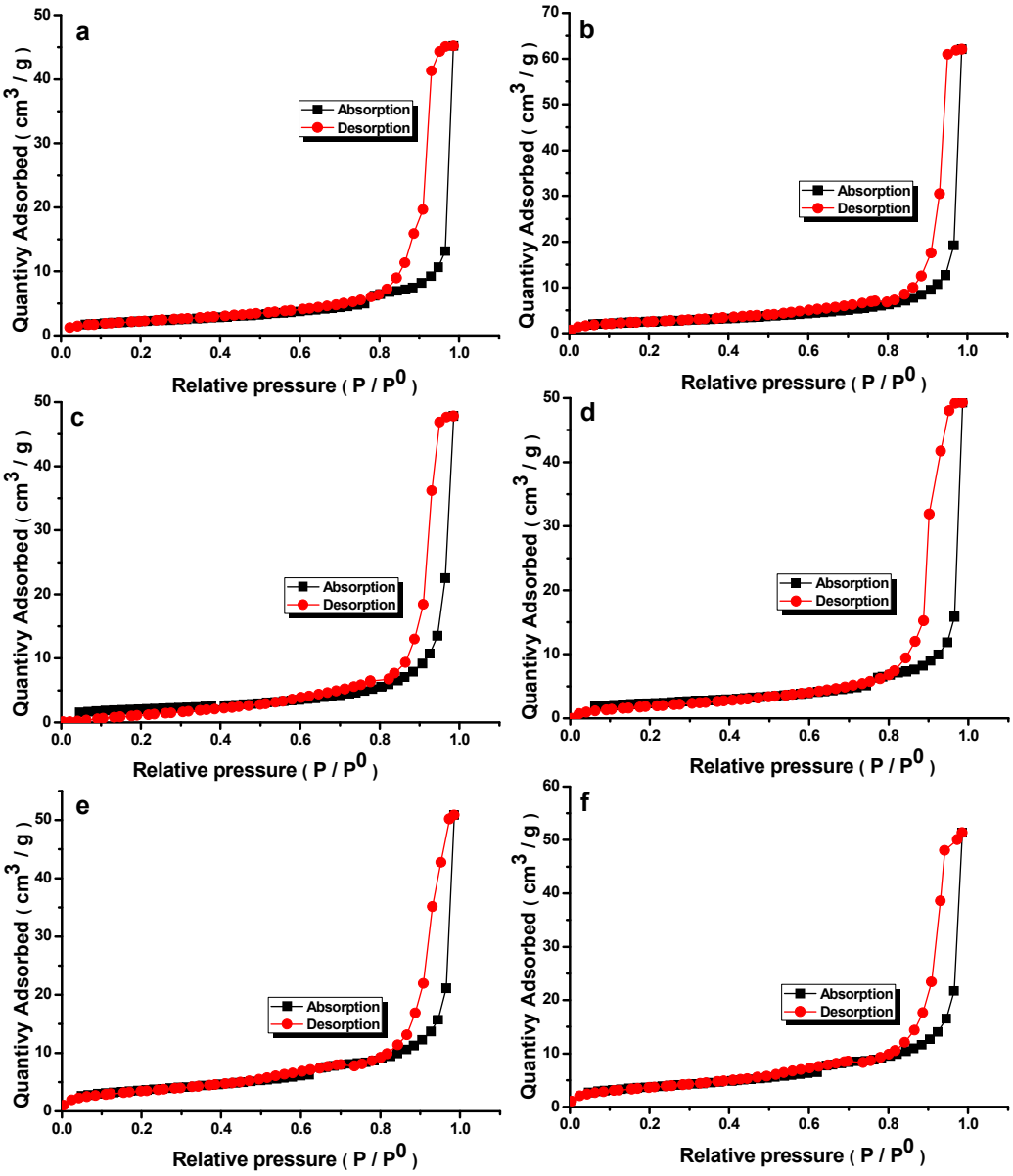

525

526 **Fig. 5** Nitrogen adsorption-desorption isotherms of the Ppy/cellulose composites, (a)

527 CPy-001, (b) CPy-002, (c) CPy-003, (d) CPy-004, (e) CPy-005and (f) CPy-006.

528

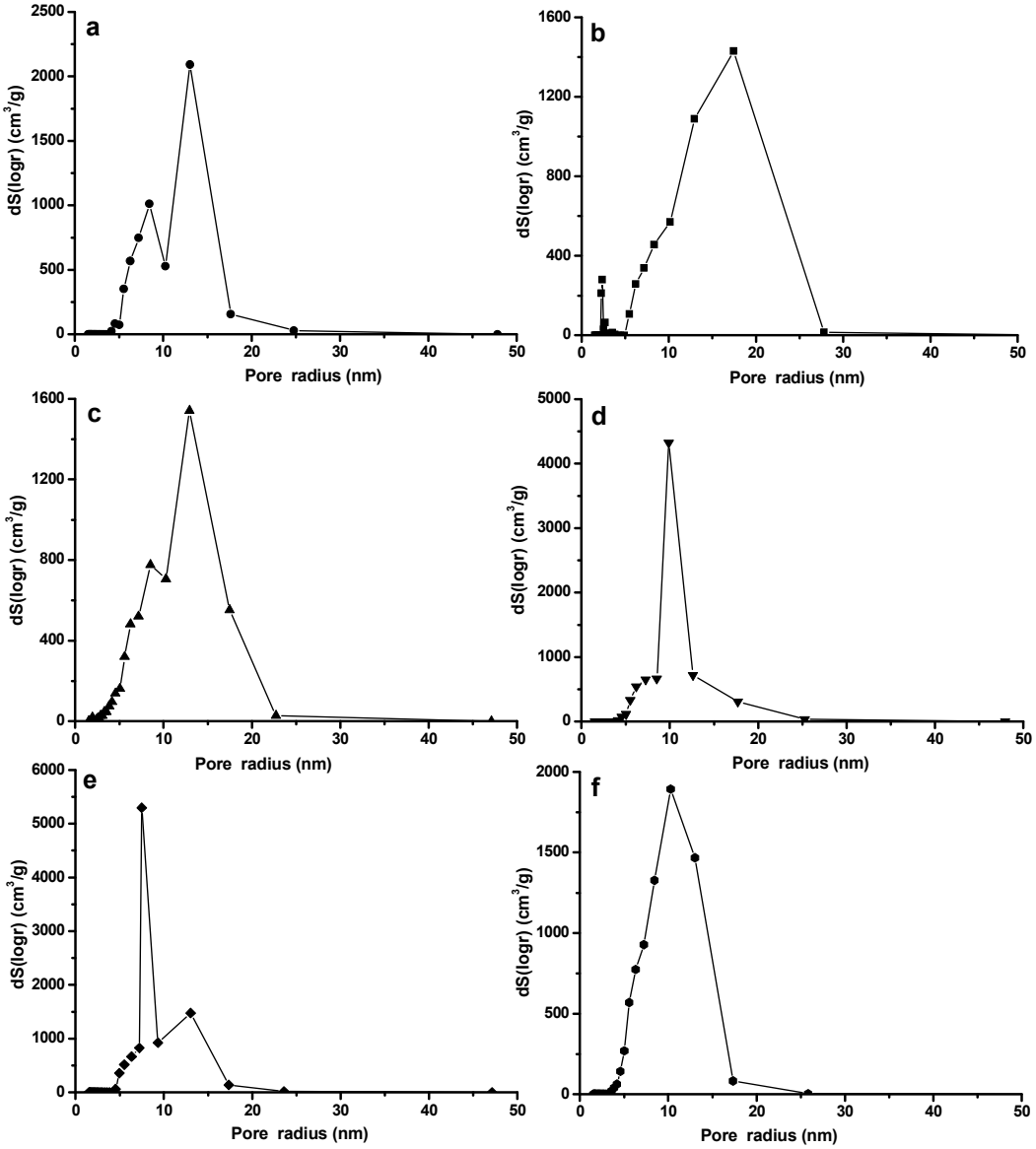

529

530 **Fig. 6** BJH pore size distribution obtained from the nitrogen adsorption-desorption
531 isotherms of the Ppy/cellulose composites, (a) CPy-001, (b) CPy-002, (c) CPy-003, (d)
532 CPy-004, (e) CPy-005 and (f) CPy-006.

533

534

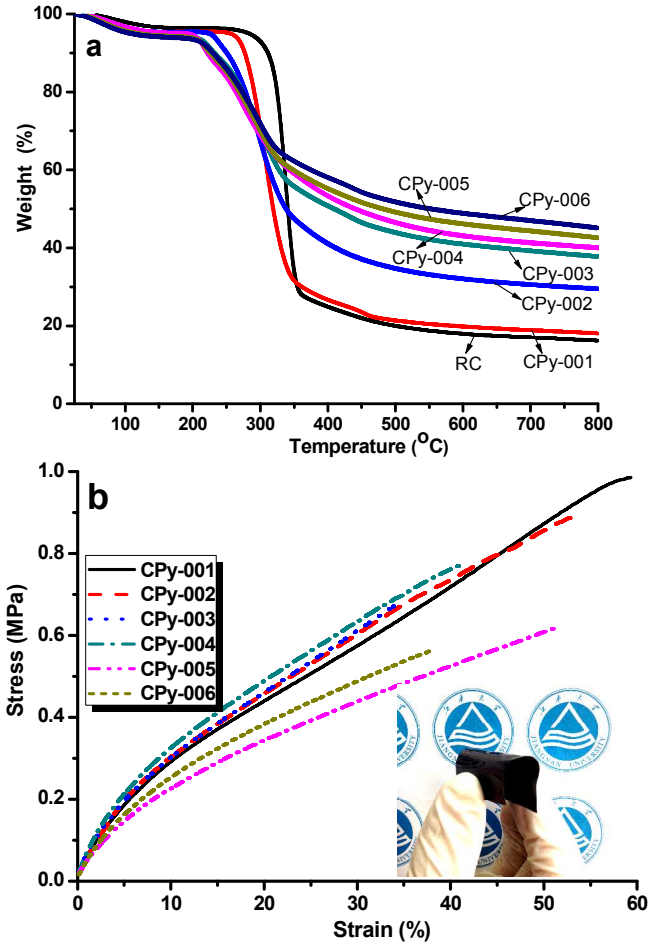

Fig. 7 TG curves of the RC and Ppy/cellulose composites(a), and tensile stress-strain curves of the Ppy/cellulose composite (b), insert was the photo of the CPy-005.

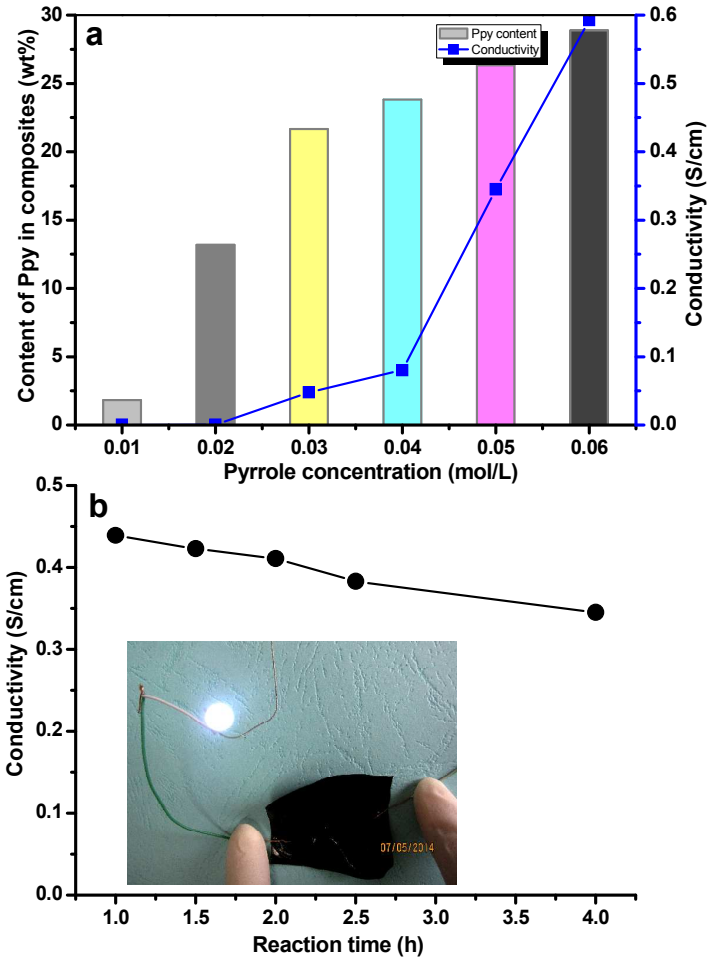

Fig. 8 Effect of the concentration of pyrrole on the content of the resulted Ppy in the composite and the conductivity of the composites (a), different polymerization time (b), and different types of dopant on the electrical conductivity of the PANI/RC composite films, inserted was the conductive test photo of the composite film prepared from aniline with concentration of 0.06 mol•L^{-1}.

548

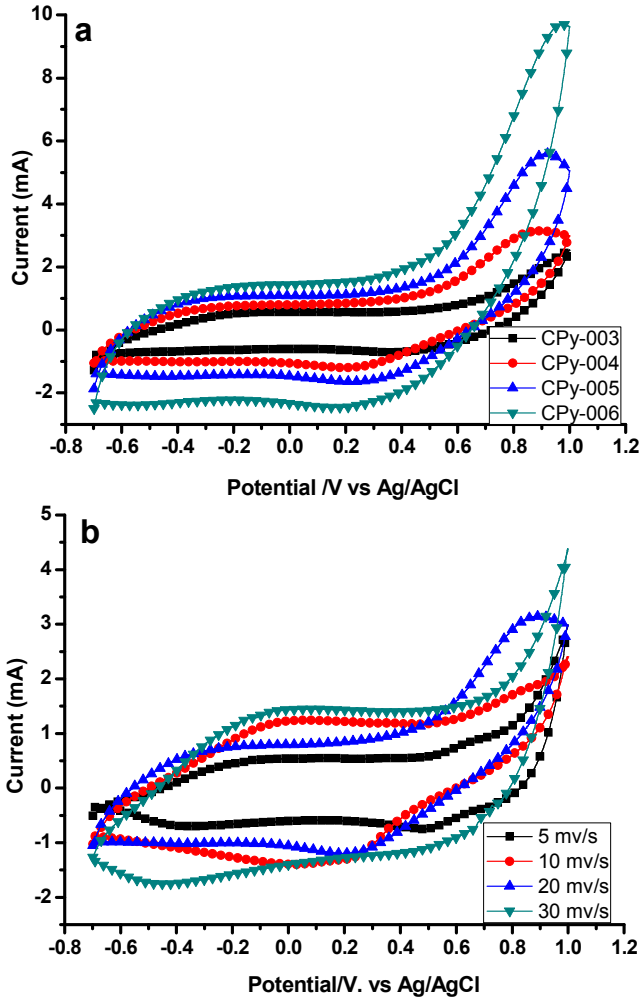

549

550 **Fig. 9** Cyclic votammograms of the Ppy/cellulose composites prepared from reaction
551 time about 4 hours at scan rate of 20 mV• s^{-1} (a), and the CPy-003 at different scan
552 rates in 1.0 mol•L^{-1} NaCl electrolyte (b).

553

554

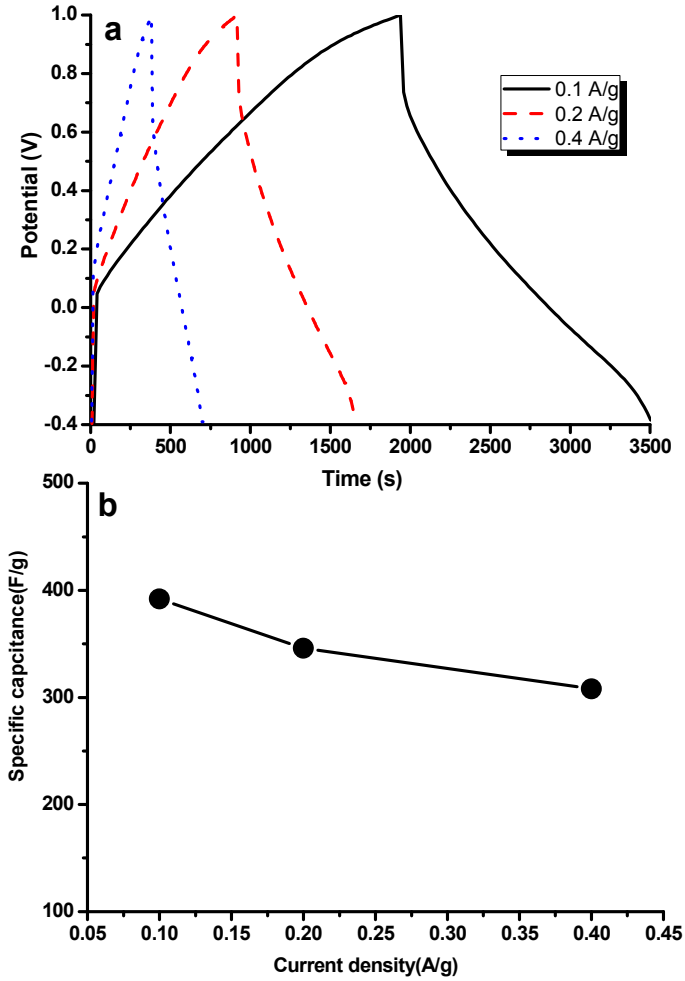

555

556 **Fig. 10** Galvanostatic charge/discharge curves of CPy-005 prepared from reaction
557 time about 4 hours at different current densities (a), and the corresponding discharge
558 capacitances of CPy-005 electrode at various current densities (b).

559

560

561

562

563

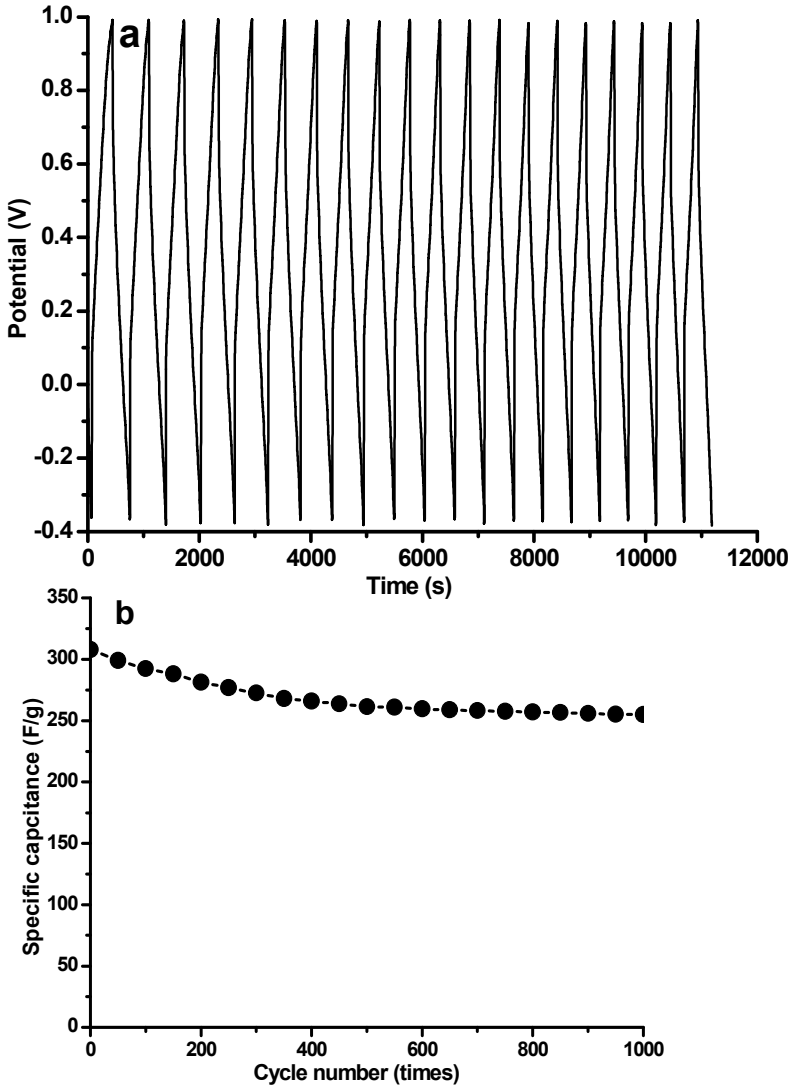

564

565 **Fig. 11** Galvanostatic charge–discharge tests (a) and cyclic performance (b) of the
566 electrode of CPy-005 prepared from reaction time about 4 hours in 1.0 mol•L^{-1} NaCl
567 solution within the potential window of -0.4-1.0 V at a current density of 0.4 A• g^{-1}.

568